PNAS
www.pnas.org

Supplementary Information Appendix for

African biomass burning is a substantial source of phosphorus deposition to the Amazon, Tropical Atlantic Ocean, and Southern Ocean

Anne E. Barkley[1], Joseph M. Prospero[1], Natalie Mahowald[2], Douglas S. Hamilton[2], Kimberly J. Popendorf[1], Amanda Oehlert[1], Ali Pourmand[1], Alexandre Gatineau[3], Kathy Panechou-Pulcherie[3], Patricia Blackwelder[1,4], Cassandra J. Gaston[1,*]

[1]Rosenstiel School of Marine and Atmospheric Sciences, University of Miami, Miami, FL, 33149

[2]Department of Earth and Atmospheric Sciences, Cornell University, Ithaca, NY, 14853

[3]ATMO Guyane, Remire-Montjoly, Guyane, France

[4]Center for Advanced Microscopy, Department of Chemistry, University of Miami, Miami, FL, 33124

*Corresponding author: cgaston@rsmas.miami.edu; Ph.: (305) 421-4979

www.pnas.org/cgi/doi/10.1073/pnas.1906091116

This PDF file includes:

Supplementary information (SI) text in Section 1 and SI Appendix Fig. S1a and S1b

Supplementary methods in Section 2

SI Appendix Figs. S2 to S14 referenced in main manuscript in Section 3

Supplementary references for SI reference citations

Supplementary Information Text

In section 1, the field site in Cayenne is described. Section 2 provides a detailed explanation of the methods and materials used during this experiment to measure dust and total phosphorus (TP) and soluble phosphorus (SP). In Section 3, the SI figures referenced in the main manuscript are shown and a detailed method of the two model approaches used to estimate the total and soluble P deposition to the Amazon and to the global ocean is given.

1. Description of field site

The blue balloon in Figure S1a shows where Cayenne, French Guiana is located in relation to South America and Africa. Cayenne is the capital of French Guiana with a population of about 60,000 in the city proper and about 125,000 in the metro area. French Guiana (4.92°N, 52.31°W) has a tropical climate that is characterized by a long, wet season from about December to June, which coincides with Saharan dust transport to South America. The country of French Guiana is a Department of France and maintains the same air quality standards as mainland France. As such, the air quality agency ATMO-Guyane (https://atmo-guyane.org/) was established to monitor air quality throughout the country. They maintain a suite of air quality monitoring equipment, including the Thermo Scientific Tapered Oscillating Microbalance (TEOM) models 1400ab and 1400-FDMS used to quantify PM_{10}, which is measured every 15 minutes and used to calculate a 24 h daily average starting at midnight local time.

PM_{10} measurements collected in Cayenne have been compared to measurements made outside the city in rural areas to assess the influence of local city emissions on PM_{10} concentrations. Minimal differences in PM_{10} concentrations were found across the sites, which suggests that the PM_{10} measurements made in Cayenne are representative of long-range transported aerosol and not from local anthropogenic emissions (1). Fig. S1b shows the high-volume sampler used to collect aerosol filter samples in the foreground and the Atlantic Ocean in the background.

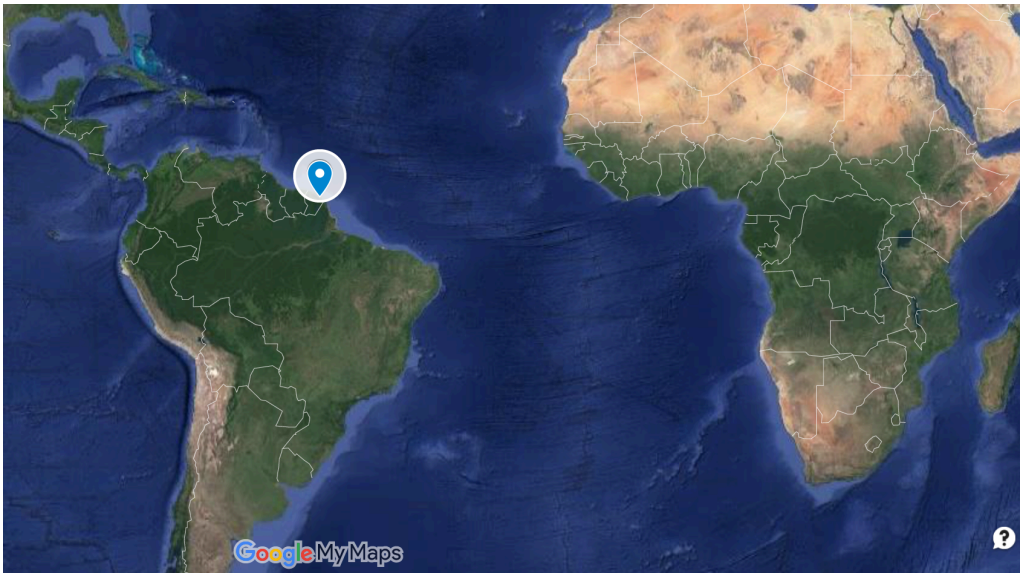

Fig. S1a. Map showing the approximate location of the field site in Cayenne, French Guiana.

Figure S1b. A photo of the University of Miami high-volume sampler atop of our sampling site, a 67-m coastal hill northeast of Cayenne. The filter is placed in the elevated cassette holder located at the far end of the sampler box; it is protected from rain by a polycarbonate "hat".

2 Aerosol collection methods

2.1 Filter Sample Collection

High-volume aerosol samples were collected almost daily (excluding weekends and French federal holidays) in 2016. Samples were collected on 20 cm x 25 cm Whatman-41 (W-41) cellulose filters with an air flow rate of approximately 0.75 m^3 min^{-1}. Samples were changed at about 10 in the morning. At the end of each cycle, the filters were then placed in individual plastic bags and

64 periodically shipped to the University of Miami for analysis along with twice monthly collected
65 procedural blanks.

66 **2.2 Dust mass concentration**

67 One-quarter of the filter was separated from the rest of the filter for dust mass concentration
68 analysis. The filters were handled only in a laminar flow hood with gloves. Each filter section was
69 washed three times with 20 mL total of Milli-Q water (Milli-Q; Millipore, resistivity > 18.2 MΩ)
70 to remove soluble compounds, such as sea salt. The washed filters were then placed in a muffle
71 furnace for 24 hours at 500°C. The residue leftover after heating is referred to as "ash" which is
72 comprised of the filter residue and non-combustible mineral matter. Procedural blanks were also
73 run with each batch of samples and the average weight of the blank was 0.13 mg, which is roughly
74 equivalent to 0.1 mg m^{-3}. The blank was subtracted from the total mass of the ash and the difference
75 is attributed to mineral dust. During the extraction and heating processes, there is some loss of
76 soluble soil minerals; therefore, an adjustment factor of 1.3 was applied to the filter ash to
77 determine the final dust mass (2). The elemental composition of western Atlantic African dust
78 determined in this way yielded an average Al concentration of 8%, close to that in the Earth's crust
79 (3). Similarly, a large suite of elements was found to be present in ratios close to average crustal
80 abundances (3, 4).

81 **2.3 Soluble Reactive Phosphorus (SRP) quantification**

82 In this paper, SP and SRP are used interchangeably. For SRP analysis, one-eighth of the
83 W-41 filter was not washed and was instead leached in 45 mL of Milli-Q buffered with sodium
84 bicarbonate ($NaHCO_3$; Sigma-Aldrich, 99.5% purity) to a pH of 7, vigorously shaken, and placed
85 in a dark room at room temperature (5–7). After 16 hours of leaching, the samples were then
86 filtered with a 0.2 μm polyethersulfone syringe filter (Whatman Puradisc), 1 mL arsenate reagent
87 was added followed by 1 mL of the molybdenum reagent. The colorimetric response of the sample

was determined at a wavelength of 880 nm in a spectrophotometer (Shimadzu UV-1800) (8) in a 1 cm cuvette. The full method can be found in Strickland and Parsons (9) including the arsenate correction (10). Standards were first analyzed in the sodium bicarbonate buffered aqueous solution at a pH = 7 using potassium monobasic phosphate to check recovery. Procedural blanks were also leached in the buffered solution and always reported as an SRP concentration below the limit of detection. All reagents were ACS reagent grade. For SP the average standard deviation was 0.7 ng m^{-3}.

2.4 Total Phosphorus (TP) quantification

One-eighth of the W-41 filter was heated to 500°C for 24 hours prior to measuring TP. The filter section was not washed in order to preserve any soluble forms of P on the filter. The dust samples were weighed and then digested with a 3:1:1 ratio of concentrated hydrochloric acid (HCl), concentrated hydrofluoric acid (HF), and concentrated nitric acid (HNO_3) in a sealed Teflon Savillex vial on a hotplate heated to 195°C for ~72 hours (5). All acids were ACS trace metal grade. The vials used for this analysis were precleaned with 2 mL of concentrated nitric acid, capped, placed on a hot plate for 4 hours at 180°C, rinsed with Milli-Q, and dried in a laminar flow hood inside a clean room. After digestion, 100 μL of the sample solution was added to 10 mL of 6 M nitric acid for analysis.

Three mineral standards (AGV-2, W2-A, and BCR-2) were also tested to ensure that the method resulted in complete digestion of refractory forms of P. All mineral standards were supplied by the United States Geological Survey (USGS). One sample was run in triplicate to investigate the reproducibility of the digestion method resulting in a standard error of 6%. The procedural blank resulted in a background level of ~1 ppm of P that was subtracted from our final sample results.

All samples and standards were analyzed by a Thermofisher Scientific Neptune Plus multi-collection inductively coupled plasma mass spectrometer (MC-ICP-MS) at the Neptune Isotope Lab (NIL) at the University of Miami. Every sample was bracketed with measurements of a standard solution to ensure accurate detection of instrument drift (11, 12). Detection of P was measured at mass-to-charge (m/z) of 30.965 amu. For TP, the average standard deviation was 6.3 ng m^{-3}.

2.5 Scanning electron microscopy (SEM)

A ~1 cm x 1 cm piece of filter was cut and placed on an aluminum SEM stub for SEM analysis. The samples were then coated with palladium in a Cressington-108 Sputter Coater and imaged with a Phillips XL-30/ESEM-FEG at 20kV at the Center for Advanced Microscopy at the University of Miami.

3. SI figures referenced in the main manuscript

3.1. Contributions of P from African dust transported to Cayenne in Spring

Filters collected in Cayenne, French Guiana were analyzed for dust mass concentration, SP concentration, and TP concentration in Spring and Fall. Fig. S2 presents the results of all measurements made at Cayenne in 2016. The filter analyses of dust are shown in red and the

128 TEOM PM_{10} (particulate matter with an aerodynamic diameter < 10 micrometers) in black.

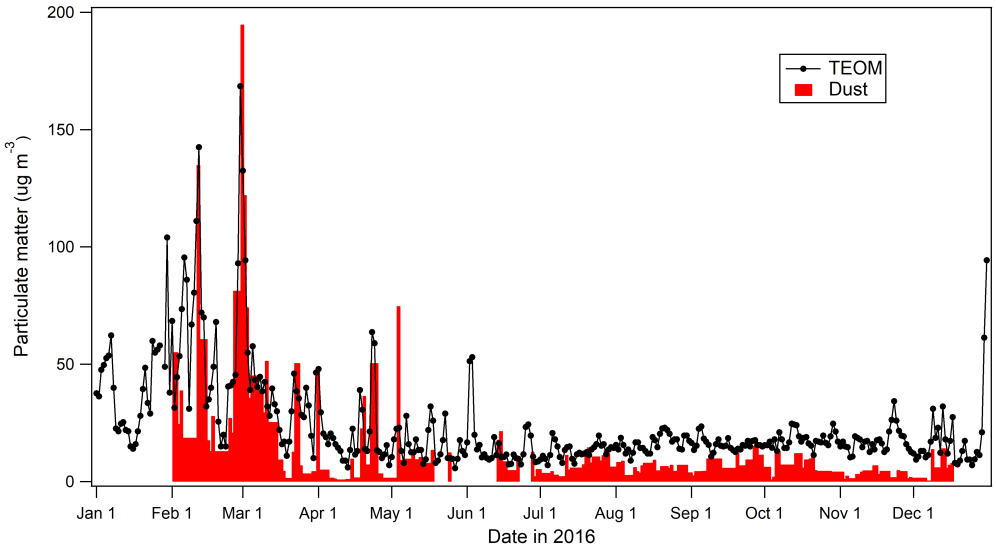

129

130 **Fig. S2**. Temporal variability of PM_{10} concentrations, shown in black, and observed dust
131 concentrations in red.

132 Fig. S3a-b below show the correlation between TP and dust as well as SP and dust for
133 Spring. P solubility of transported dust was determined for Spring by taking the average solubility
134 of major dust events (e.g., > 50 μg m^{-3}), which yielded an average P solubility of 5%.

135 The Scanning electron microscopy (SEM) images in Fig. S4 show the presence of biomass
136 burning (BB) aerosol and mineral dust from the Saharan Desert co-transported to Cayenne in the
137 Spring. This image is representative of filter images of samples collected in February and March
138 when elevated SP concentrations were measured in Cayenne. Fig. S5 shows photos of the filters.
139 The co-transport of BB emissions and dust is also indicated by the color of the filter as well. While
140 typical dust-laden filters are reddish-orange, these filters are grey-brown, which is indicative of
141 mineral dust and black carbon from BB emissions. The color of the filters shown in Fig. S5 is
142 representative of typical filters collected in February and March. Figs. S6a-c show thermal
143 anomalies detected by the Visual Infrared Imaging Radiometer Suite (VIIRS), which indicate fire
144 activity in a region. From this figure, it is evident that fire activity is prevalent in the Sahel in

February and March, but decreases in April in 2016. Fire data was obtained by the Fire Information Resource Management System (FIRMS; https://firms.modaps.eosdis.nasa.gov/).

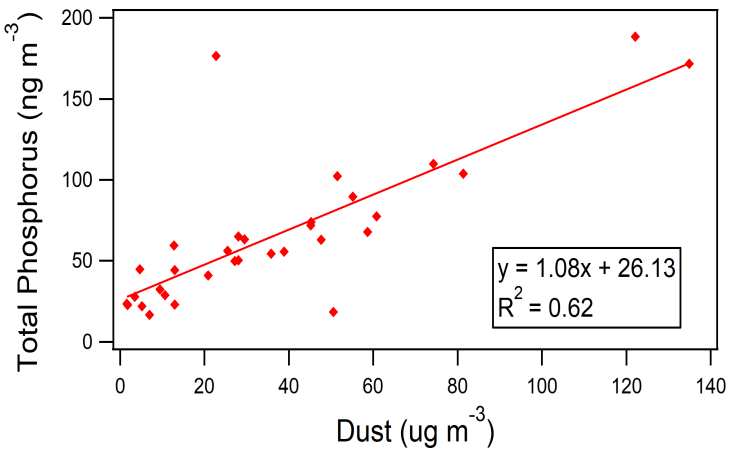

Fig. S3a. Correlation for dust and total phosphorus for data from Feb to Apr (Spring) 2016.

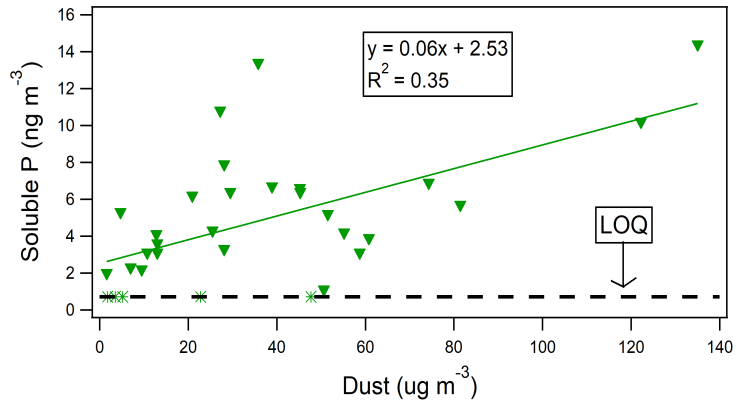

Fig. S3b. Correlation plot for dust and soluble phosphorus for data from Feb to Apr (Spring) 2016. The LOQ is also shown as a black dashed line and has a value of 0.71 ng m^{-3}. This plot is different from that in Fig. 1c in the main manuscript because it includes the points that were at or below the LOQ.

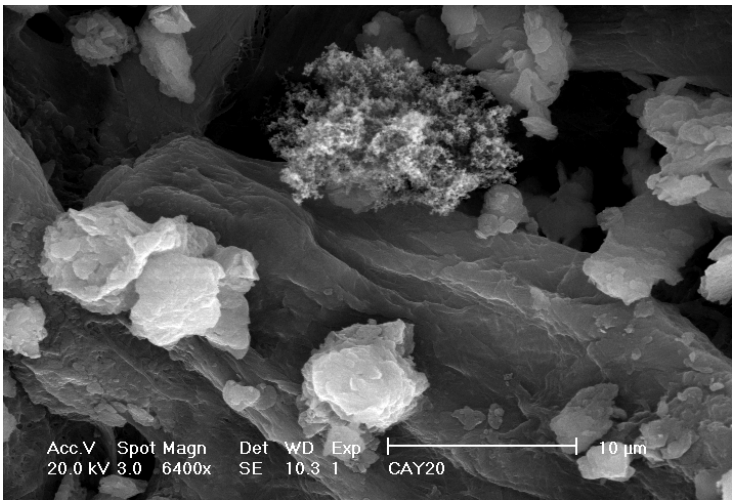

Fig. S4. SEM image showing transported biomass burning aerosol in the upper right and mineral dust in the lower left on the same filter from February 2016. The scale bar is on the bottom and represents 10 µm.

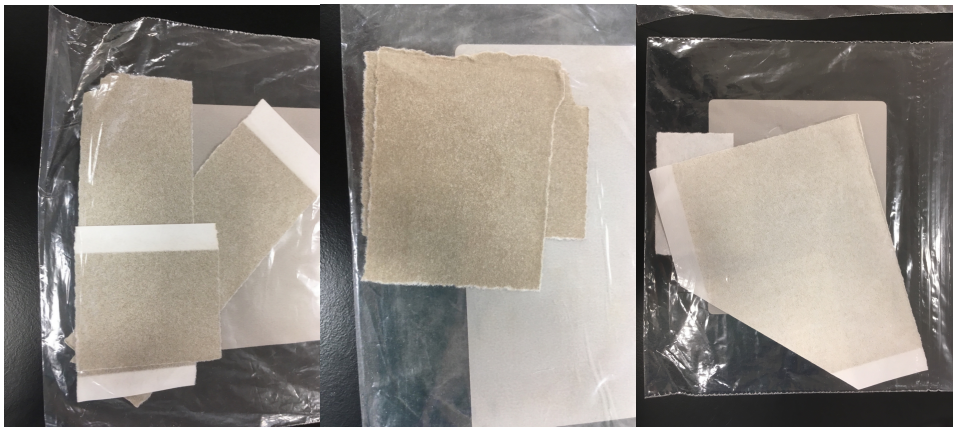

Fig. S5. Filters collected in Cayenne on 01, 5, and 17 February 2016 (left to right) showing grey-brown hue indicative of co-transported black carbon from biomass burning emissions in the Sahel and mineral dust.

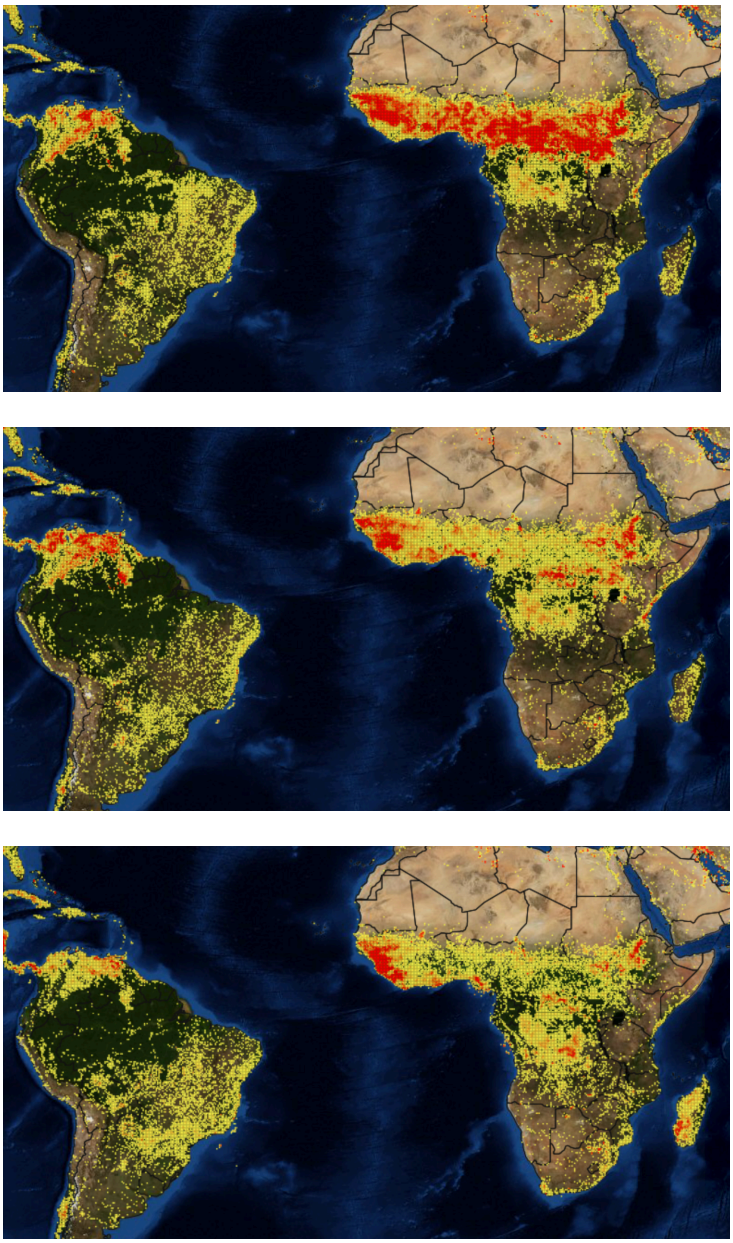

Fig. S6a-c. The red and yellow colors in Africa shows fire activity in the Sahel in February (top), March (middle), and April (bottom) 2016. The fire intensity scale is gradational with red denoting greater fire activity and yellow denoting less fire activity.

3.2. An additional supply of P from southern African BB in Fall

Fig. S7 shows BB aerosol imaged by SEM that was transported to Cayenne in Fall likely from southern Africa. Fig. S8 shows the medium grey color of filters collected in September; the grey hue is from black carbon associated with biomass burning and is representative of all filters collected in Fall.

Fig. S9 shows the correlation in Fall between dust and SP. From Fig. S9, the relationship between SP and dust is poorly correlated in Fall and many values of SP in late Oct and Nov are below the LOQ. Fig. S10a shows a time-series of SP data collected in Fall and Fig. S10b shows a 13-day air mass back trajectory initiated on 3 October 2016 when the SP concentration is below the LOQ. Figs. S10c-e show the vertical profiles of the air masses as they are transported across the Atlantic Ocean. The boxed points in Fig. S10b correspond to the vertical air profiles in Fig. S10c-e. This figure shows that on days when SP was measured to be below the LOQ, there is no smoke transport to Cayenne.

SI Fig. S11 shows an air mass BT frequency plot initialized on 1 November 2016 and run every 6 hours to give a spatial distribution of where air masses come from during the month of November. This figure shows that the air masses no longer originate from southern Africa in November. Indeed, the air masses typically come from either the nation of South Africa or from near the equator.

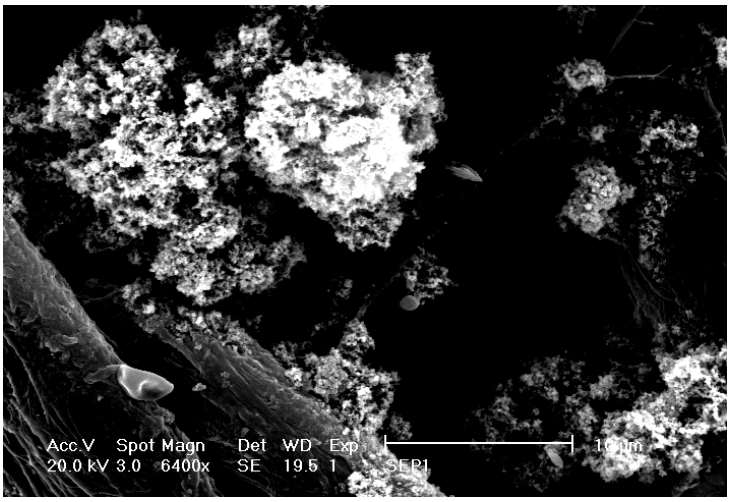

Fig. S7. Scanning election microscopy image showing numerous biomass burning particles on filters collected in Cayenne in September 2016. The scalebar is on the bottom and represents 10 µm.

Fig. S8. Filters collected in Cayenne on 05, 16, and 23 September 2016 (left to right) showing a grey hue indicative of biomass burning emissions transported to Cayenne.

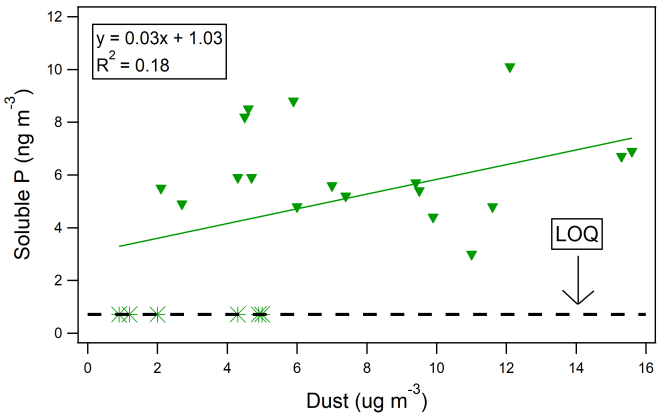

201

202 **Fig. S9.** Correlation plot for dust and soluble phosphorus for data from Sept to Nov (Fall) 2016.

203 The LOQ is also shown as a black dashed line and has a value of 0.71 ng m^{-3}. Most values below

204 the LOQ are from late Oct and Nov.

205

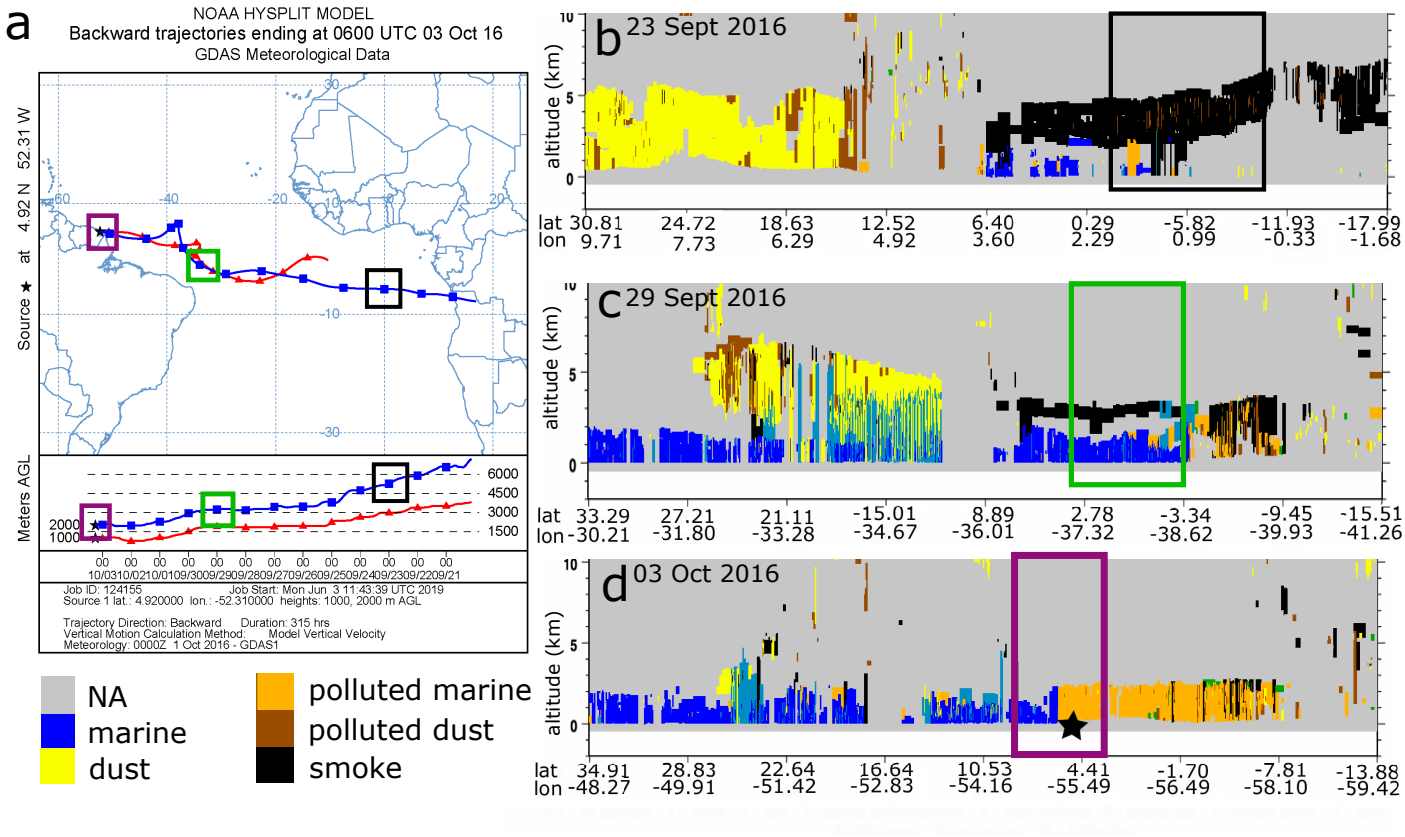

206

207 **Fig. S10.** This figure is similar to Fig. 3 in the main manuscript except this figure shows the

208 progression of elevated smoke on a day without measurable SP. The black arrows on the aerosol

vertical profiles show the approximate intersection of the BT to the CALIPSO pass. From S10d, it is evident that the smoke plume is thin within a narrow altitude band. The purple box in S10e emphasizes the lack of an elevated smoke layer when the air BT intersects Cayenne. The black stars show the location of Cayenne.

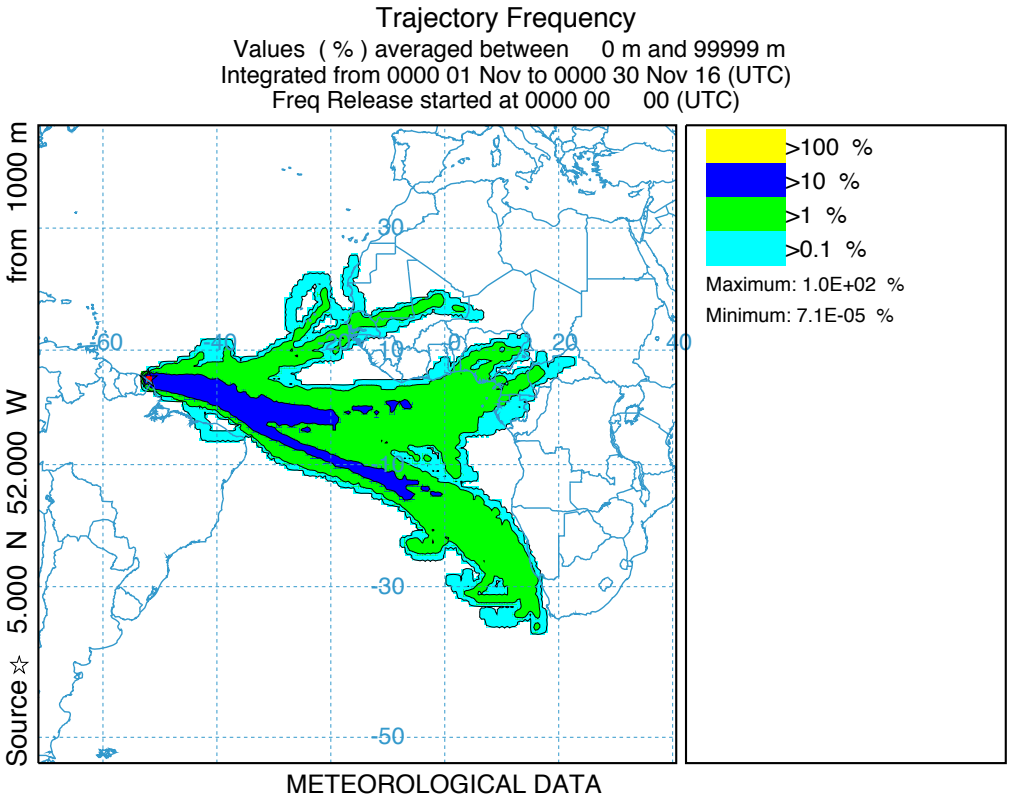

Fig. S11. Air mass BT frequency plot initialized on 1 November 2016 and run every 6 hours for the month of November.

3.3. Estimates of P deposition to the Amazon using the MERRA-2 model and CAM biogeochemical model

3.3.1 Using the MERRA-2 model to estimate P deposition to the Amazon

Fig. S12 shows a frequency plot of 96-hour forward trajectories using the HYSPLIT model initialized at 500 m from 1 February to 30 April 2016 every 6 hours. This figure shows that after air masses arrive in Cayenne, they typically continue into the interior of the Amazon, which demonstrates that Cayenne intercepts air masses upwind of the Amazon Basin.

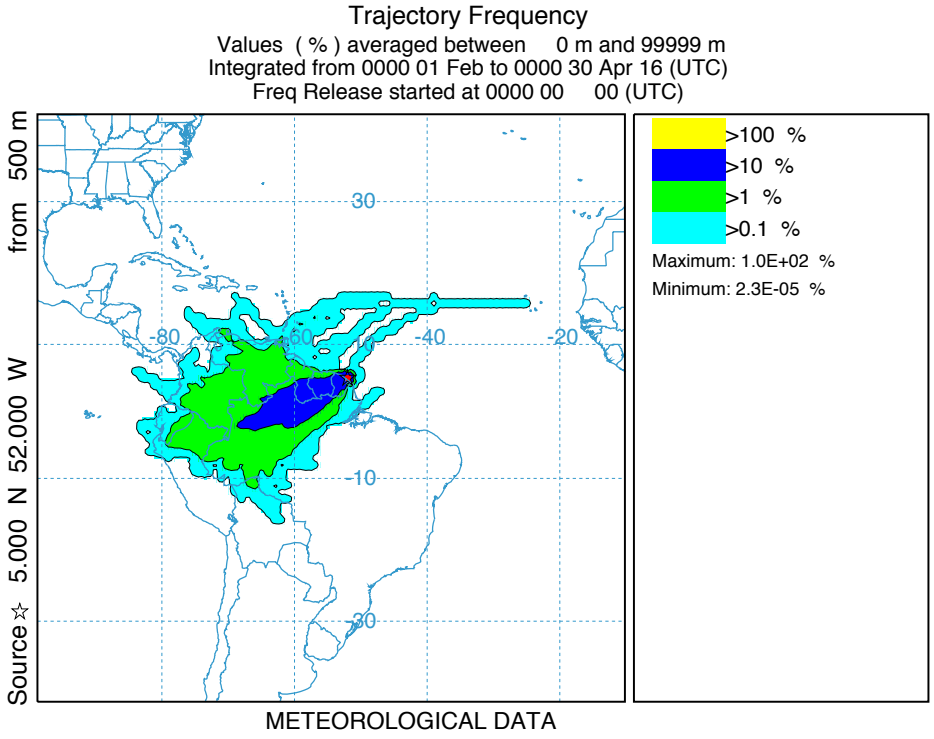

Fig. S12. Ninety-six-hour air mass forward trajectories initialized at 500 m on 1 February 2016 to 30 April 2016 every 6 hours showing that air masses originating in Cayenne typically continue into the interior of the Amazon Basin.

We first discuss our approach using the MERRA-2 model to estimate P deposition from African dust. The MERRA-2 model is based on the GEOS-5 Earth System model coupled to the GOCART aerosol module (13). Version 2 performance has been substantially improved by assimilating aerosol optical depth (AOD), primarily MODIS since 2002. Comparisons of

MERRA-2 surface aerosol model products with in situ measurements at sites in the United States show that the model provides consistently accurate estimates during African and Asian dust events (14). MERRA-2 also yielded excellent agreement with Barbados monthly means over the period 1984 – 2009 (13, 15). Fig. S13 shows the MERRA-2 model output of monthly dust mass concentration for Cayenne, represented by the coordinates: -52.5°W to -51.5°W and 4.5°N to 5.5°N, and measured dust mass concentration from our site in Cayenne. There was considerable agreement between our dust observations and the model output in both the magnitude and seasonal transport pattern to Cayenne. The MERRA-2 model captured the increase in dust in the Spring (February to May) when dust is transported from the Sahara to South America.

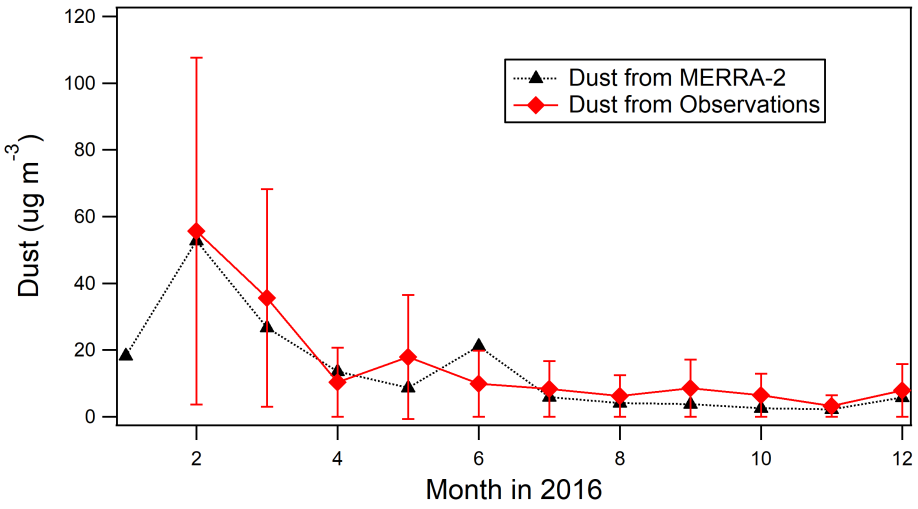

Fig. S13. Monthly average dust concentrations measured at Cayenne and monthly average dust estimates from MERRA-2 for 2016. The error bars in red are monthly standard deviations for our measured dust mass concentrations. MERRA-2 results were obtained from https://giovanni.gsfc.nasa.gov/giovanni/.

The MERRA-2 deposition product yielded a deposition rate of 4 g m^{-2} a^{-1} for the Cayenne region. The only directly measured dust deposition data in the western Atlantic is that for Florida where rates were in the range of 1.5 to 2.0 g m^{-2} a^{-1} (16). The MERRA deposition rate for Cayenne

is comparable to Holocene deposition rates to the central tropical North Atlantic, 1 – 5 g m^{-2} a^{-1}. (17). An extensive study by Kienast et al. (18) of dust input rates to the oceans using the Thorium-232 method (Thoromap) presents data for the late Holocene (0 – 4ka) in sediments off the NE coast of SA directly east of Cayenne. These yield rates of 2 – 4 g m^{-2} a^{-1} and 4 – 8 g m^{-2} a^{-1}. Thus, the MERRA-2 rates obtained for Cayenne fall in the mid-range of those measured in regional sediment cores.

We estimated the amount of TP deposited by African dust over the entire Amazon Basin using monthly wet and dry dust deposition rates obtained from the MERRA-2 model over three quadrants representative of the Amazon Basin (-75°W, 2°S, -50°W, 8°N), (-75°W, 12°S, -50°W, 2°S), and (-50°W, 12°S, -40°W, 2°S), as prescribed by Yu et al. (19). Using a TP to dust ratio of 1080 ppm (SI Fig. S3a), the TP deposition associated with wet and dry dust deposition was found. This yielded a TP deposition of 0.011 Tg TP yr^{-1} for the Amazon. Our TP deposition estimates for African dust are within the range of Yu et al. (2015).

3.3.2. Using the CAM model to estimate P deposition to the Amazon and the Oceans

The second way that deposition was calculated was with version 4 of the Community Atmospheric Model (CAM) using the model simulations separating each source (dust and BB separately from Africa) as previously described (14). CAM has been used previously to estimate P deposition to the Amazon Basin (20). For the P deposition estimates to the Amazon shown in Table 1, the CAM model was tuned to match the P observations at Cayenne. For Figs. 4, 5, and 6 in the main manuscript, CAM used a 2.5° x 1.9° horizonal (longitude by latitude) resolution and 56 vertical layers up to 2 hPa. This version of CAM had previously been used to independently estimate iron deposition from dust and combustion sources (21). Meteorology (e.g., winds and temperature) was nudged to the Modern-Era Retrospective analysis for Research and Applications (MERRA) data for 2006-2011, and the climatological monthly mean was used in this study.

279 Sources were separated by sub-continents, and originally focused on iron, but for this study, we
280 use the source apportionment for P deposition instead.
281 To deduce the relative importance of dust and BB contributions from African sources on the
282 Amazon, we made simple assumptions about the relationship between Fe and P, based on an iron
283 content of 3.5% in dust and 1080 ppm P in dust. For biomass burning, we assume a P/BC ratio of
284 0.0029 in the submicron mode and 0.020 in the supermicron mode. The average Fe/BC in
285 combustion aerosols is assumed to be 0.2. For Fig. 4, we tuned the model to match the P
286 observations in this study (see Fig S14) by first estimating enough Fe in dust to account for the
287 observed dust mass concentrations, then converting the estimated Fe to P. To match our
288 observations, we increased the dust by 2-fold to match the P and soluble P for the boreal winter
289 months (see Figure S14a). To match our observations particularly in Fall when BB dominates,
290 current P/BC ratios alone cannot explain our P observed, and we needed to increase our P from
291 combustion by 60-fold (Figure S14b). This required enhancement can be due to a combination of
292 factors: larger aerosol emissions from biomass burning than estimated by the biomass burning
293 inventory (consistent with previous comparisons with AERONET, which required an
294 enhancement by a factor of 3 in Africa from local observations (22)), higher P emissions from
295 biomass burning than predicted by currently used P/BC ratios, or inadequate transport from Africa
296 to South America in the model. Finally, we use a SP fraction for dust and combustion of 0.05 and
297 0.15, as deduced in this study, for the deposition. The bulk (>80%) of the combustion aerosol
298 simulated in the model from the North African and South African sources is from biomass burning
299 not industrial sources. An estimate of the uncertainty in these estimates would suggest that for the
300 dust P, using the original model simulations, which were tuned to match local source strength in
301 North Africa would be a good lower bound, while tuning to the observations here (multiplying by
302 a factor of 2), would be the upper end estimate. For the biomass burning, since local observations

303 from AERONET suggest that the wildfire emissions should be multiplied by a factor of 3x (23),
304 we include this as a lower end estimate, while the higher value (multiplied by a factor of 60x) to
305 match the observations here, are used as an upper end. This gives us a range from 0.011-0.033 Tg
306 P yr^{-1} of total P and 0.0006 to 0.002 Tg P yr^{-1} in SP from dust deposition to the Amazon, and, in
307 comparison, 0.0026-0.052 Tg P yr^{-1} of total P, and 0.0004-0.008 of SP from biomass burning
308 deposition in the Amazon.

309 For our global deposition estimates shown in Figs. 5 and 6, we used a slightly different set of
310 model runs, described in Brahney et al. (23) and Chien et al. (24) and did not tune CAM to our
311 observations since global sources rather than the local sources that were measured in this study
312 were accounted for. For these simulations, the winds were derived online, with fixed sea surface
313 temperatures. All sources of P were included (dust, sea salts, biomass burning, fossil fuels, primary
314 biogenic particles and volcanoes), but were not separated into different regional sources. The only
315 change from Brahney et al., (23) and Chien et al., (24) is that the soluble fraction was assumed to
316 be 0.05 for dust and 0.15 for other sources, as found in this study.

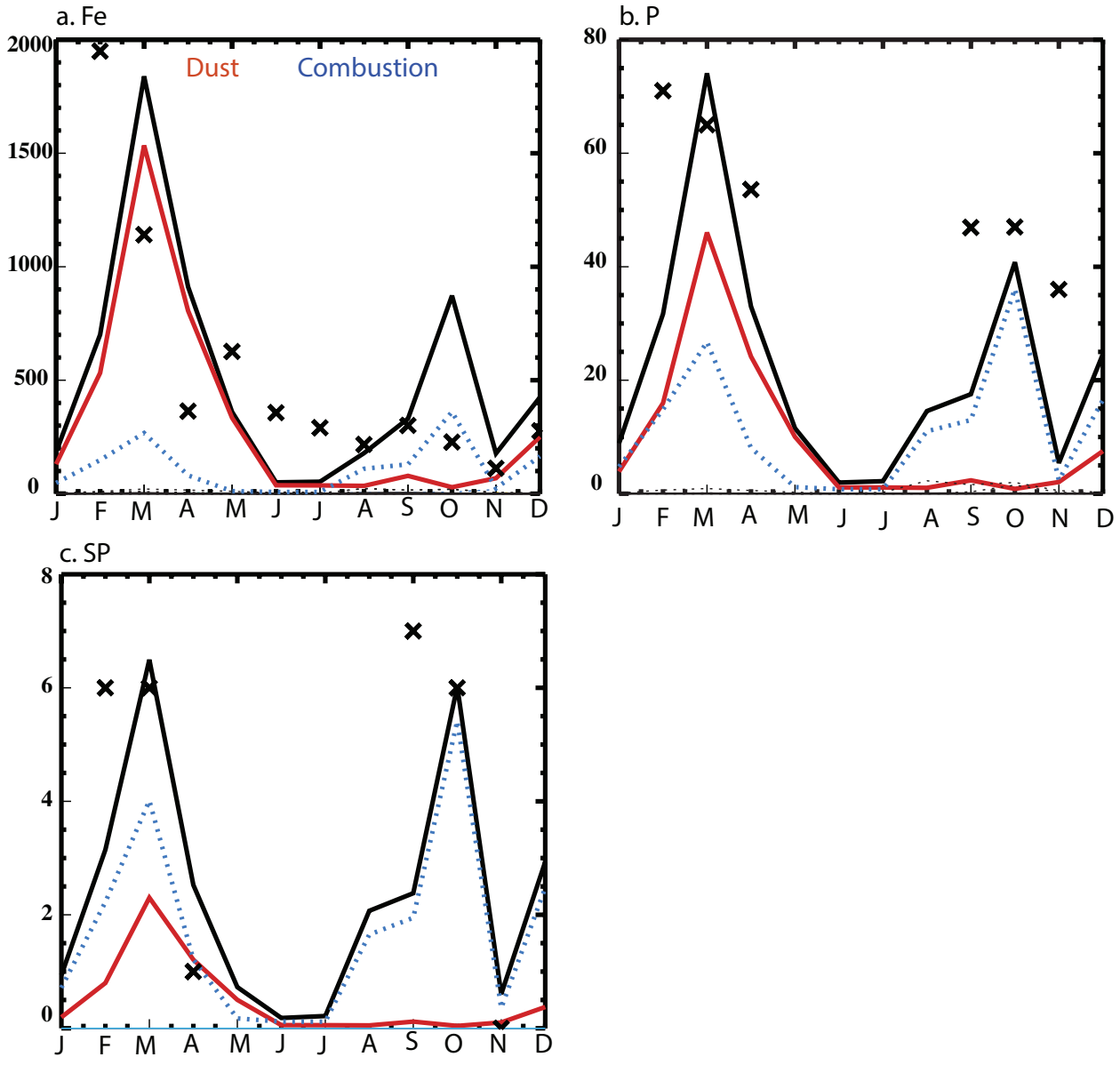

Figure S14. Model predictions from the Community Atmospheric Model (CAM) estimating the Fe (a), TP (b) and SP (c) concentrations (all in ng m^{-3}) from different sources at the Cayenne measurement site, versus the observations (black x). The different aerosol sources include African combustion (dotted blue line) and African dust (solid red line). The solid black line represents the total Fe (a), P (b), and SP (c) concentrations from both sources. Emissions of BB from within the Amazon are excluded in order to focus on the impact of long-range transported aerosol.

REFERENCES CITED

1. Prospero JM, Collard F, Molinié J, Jeannot A (2014) Characterizing the annual cycle of African dust transport to the Caribbean Basin and South America and its impact on the environment and air quality. *Global Biogeochem Cycles* 28(7):1–17.
2. Prospero JM (1999) Long-term measurements of the transport of African mineral dust to the southeastern United States: Implications for regional air quality. *J Geophys Res* 104(D13):15917–15927.
3. Trapp JM, Millero FJ, Prospero JM (2010) Trends in the solubility of iron in dust-dominated aerosols in the equatorial Atlantic trade winds: Importance of iron speciation and sources. *Geochemistry, Geophys Geosystems* 11(3):1–22.
4. Bozlaker A, Prospero JM, Price J, Chellam S (2018) Linking Barbados Mineral Dust Aerosols to North African Sources Using Elemental Composition and Radiogenic Sr, Nd, and Pb Isotope Signatures. *J Geophys Res Atmos* 123(2):1–6.
5. Baker AR, Jickells TD, Witt M, Linge KL (2006) Trends in the solubility of iron, aluminium, manganese and phosphorus in aerosol collected over the Atlantic Ocean. *Mar Chem* 98(1):43–58.
6. Zamora LM, Prospero JM, Hansell DA, Trapp JM (2013) Atmospheric P deposition to the subtropical North Atlantic: Sources, properties, and relationship to N deposition. *J Geophys Res Atmos* 118(3):1546–1562.
7. Chen Y, Street J, Paytan A (2006) Comparison between pure-water- and seawater-soluble nutrient concentrations of aerosols from the Gulf of Aqaba. *Mar Chem* 101(1–2):141–152.
8. Ridame C, Guieu C (2002) Saharan input of phosphate to the oligotrophic water of the open western Mediterranean sea. *Limnol Oceanogr* 47(3):856–869.
9. Strickland JDH, Parsons TR (1972) *A Practical Handbook of Seawater Analysis*

doi:10.1002/iroh.19700550118.

10. Johnson DL (1971) Simultaneous determination of arsenate and phosphate in natural waters. *Environ Sci Technol* 5(5):411–414.

11. Pourmand A, Prospero JM, Sharifi A (2014) Geochemical fingerprinting of trans-Atlantic African dust based on radiogenic Sr-Nd-Hf isotopes and rare earth element anomalies. *Geology* 42(8):675–678.

12. Pourmand A, Dauphas N, Ireland TJ (2012) A novel extraction chromatography and MC-ICP-MS technique for rapid analysis of REE, Sc and Y: Revising CI-chondrite and Post-Archean Australian Shale (PAAS) abundances. *Chem Geol* 291:38–54.

13. Randles CA, et al. (2017) The MERRA-2 Aerosol Reanalysis, 1980 Onward. Part I: System Description and Data Assimilation Evaluation. *J Clim* 30(17):6823–6850.

14. Chen SP, Lu CH, McQueen J, Lee P (2018) Application of satellite observations in conjunction with aerosol reanalysis to characterize long-range transport of African and Asian dust on air quality in the contiguous U.S. *Atmos Environ* 187(November 2017):174–195.

15. Buchard V, et al. (2017) The MERRA-2 aerosol reanalysis, 1980 onward. Part II: Evaluation and case studies. *J Clim* 30(17):6851–6872.

16. Prospero JM, Landing WM, Schulz M (2010) African dust deposition to Florida: Temporal and spatial variability and comparisons to models. *J Geophys Res Atmos* 115(13):1–19.

17. Kohfeld KE, Harrison SP (2001) DIRTMAP: The geological record of dust. *Earth-Science Rev* 54(1–3):81–114.

18. Kienast SS, Winckler G, Lippold J, Albani S, Mahowald NM (2016) Tracing dust input to the global ocean using thorium isotopes in marine sediments: ThoroMap. *Global*

Biogeochem Cycles 30(10):1526–1541.

19. Yu H, et al. (2015) The Fertilizing Role of African Dust in the Amazon Rainforest: A First Multiyear Assessment Based on CALIPSO Lidar Observations. *Geophys Res Lett* 42:1984–1991.

20. Mahowald NM, et al. (2005) Impacts of biomass burning emissions and land use change on Amazonian atmospheric phosphorus cycling and deposition. *Global Biogeochem Cycles* 19(4). doi:10.1029/2005GB002541.

21. Mahowald NM, et al. (2018) Aerosol trace metal leaching and impacts on marine microorganisms. *Nat Commun* 9(1). doi:10.1038/s41467-018-04970-7.

22. Ward DS, et al. (2012) The changing radiative forcing of fires: global model estimates for past, present and future. *Atmos Chem Phys* 12:10857–10886.

23. Brahney J, Mahowald N, Ward DS, Ballantyne AP, Neff JC (2015) Is atmospheric phosphorus pollution altering global alpine Lake stoichiometry? *Global Biogeochem Cycles* 29:1369–1383.

24. Chien C-T, et al. (2016) Effects of African dust deposition on phytoplankton in the western tropical Atlantic Ocean off Barbados. *Global Biogeochem Cycles* 30. doi:10.1002/2015GB005334.